Supplement of Hydrol. Earth Syst. Sci., 27, 3083–3114, 2023
https://doi.org/10.5194/hess-27-3083-2023-supplement

Hydrology and Earth System Sciences
Open Access

Supplement of

Stable water isotopes and tritium tracers tell the same tale: no evidence for underestimation of catchment transit times inferred by stable isotopes in StorAge Selection (SAS)-function models

Siyuan Wang et al.

Correspondence to: Siyuan Wang (s.wang-9@tudelft.nl)

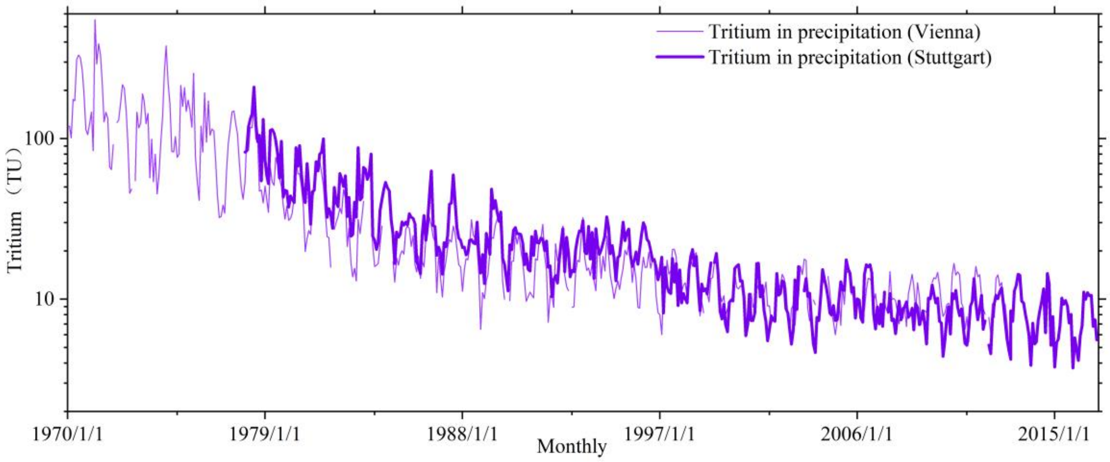

Figure S1. Long term ^3H data in precipitation at Vienna station and Stuttgart (thin violet line for Vienna station and dark violet line for Stuttgart station).

We estimated the sine wave parameters a_P, b_P and φ_P in each of the four precipitation zones (P1 – P4) based on the multiple regression coefficients reported by Allan et al. (2018) in which the study area is very closed to our catchment as follows:

$$a_P = (-7.90 * 10^{-6}) * La_P + (-2.62 * 10^{-6}) * Lo_P + 0.0006 * H_P + 0.28 * Tr_P - 0.009 * P_P - 0.43 \quad (S1)$$

$$\varphi_P = (-6.29 * 10^{-7}) * La_P + 1.82 \quad (S2)$$

$$b_P = (3.45 * 10^{-6}) * La_P + (1.19 * 10^{-6}) * Lo_P - 0.002 * H_P - 0.18 * Tr_P - 5.83 \quad (S3)$$

With La_P [°] latitude, Lo_P [°] longitude, H_P [m] elevation, Tr_P [°C] mean annual range of monthly temperatures, and P_P [cm] mean annual precipitation. Note that all of the above individual spatial predictor variables, averaged for each precipitation zone (P1 – P4) (Table S1).

Table S1 The sine parameters' predictor variables in different precipitation zones in the Neckar river basin.

Precipitation zone	La_P [°]	Lo_P [°]	Hp [m]	TrP [°C]	P_P [cm]
P1	48.42	8.87	568.04	19.90	93.28
P2	48.92	9.12	322.20	20.05	80.87
P3	49.05	9.71	420.53	20.09	88.97
P4	48.56	8.52	673.21	19.76	105.27
Stuttgart station	48.83	9.20	314.00	20.04	69.08

Table S2 The estimates of sine parameters for different precipitation zones and Stuttgart station.

	a_P [‰]	φ_P [rad]	b_P [‰]
P1	4.64	1.82	-10.55
P2	4.65	1.82	-10.08
P3	4.65	1.82	-10.29
P4	4.56	1.82	-10.73
Stuttgart	4.75	1.82	-10.06

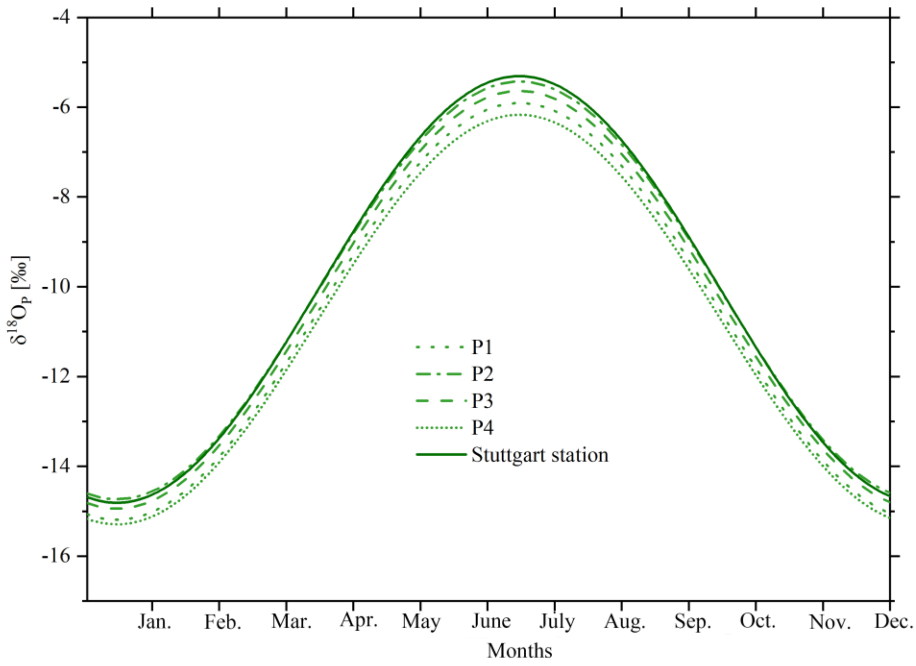

Figure S2. The $\delta^{18}O_P$ sine wave for precipitation zones (P1 – P4) and Stuttgart station.

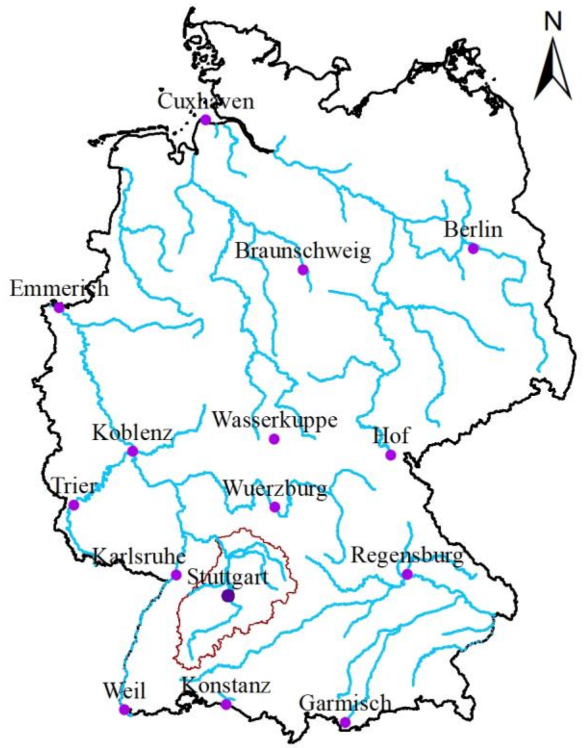

Figure S3. ^{3}H concentrations in precipitation observed at 15 multiple locations across Germany.

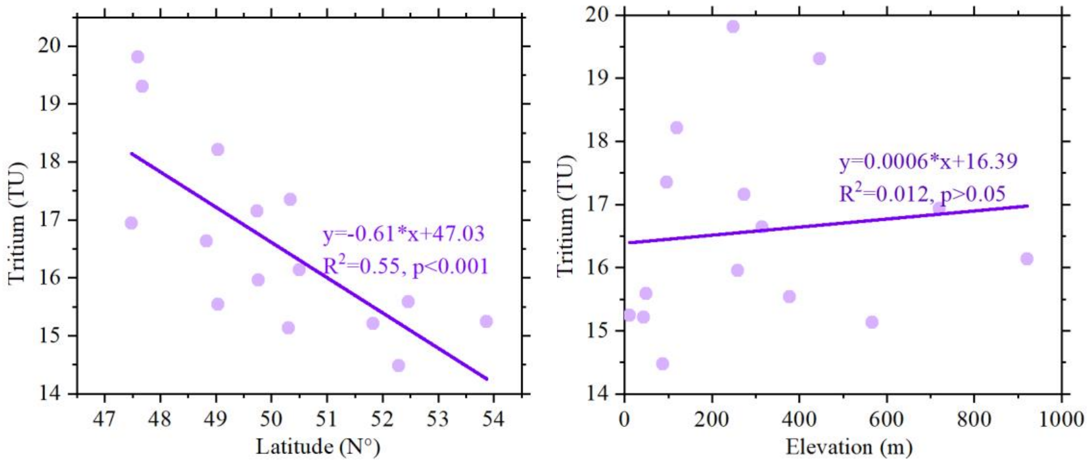

Figure S4. The linear regression relationships between ^{3}H concentrations in precipitation observed at 15 locations across Germany with latitude and elevation respectively.

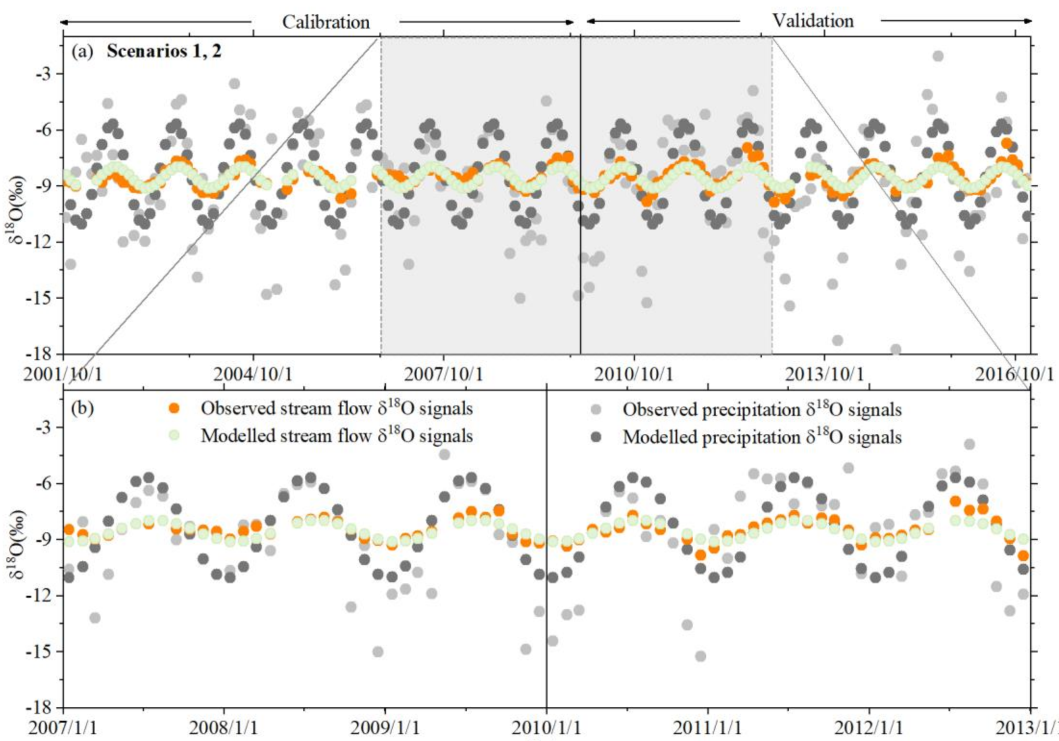

Figure S5. The time series of stream $\delta^{18}O$ reproduced by SW models, i.e., calibration strategy C_x (scenario 1, 2), for the model calibration and evaluation periods. (a) Observed $\delta^{18}O$ signals in precipitation (light grey dots) and modelled $\delta^{18}O$ signals in precipitation (dark grey dots), and observed stream $\delta^{18}O$signals (orange dots) as well as modelled stream $\delta^{18}O$signals (light green dots), (b) zoom-in of observed and modelled $\delta^{18}O$ signals for the 01/01/2007 – 31/12/2012 period.

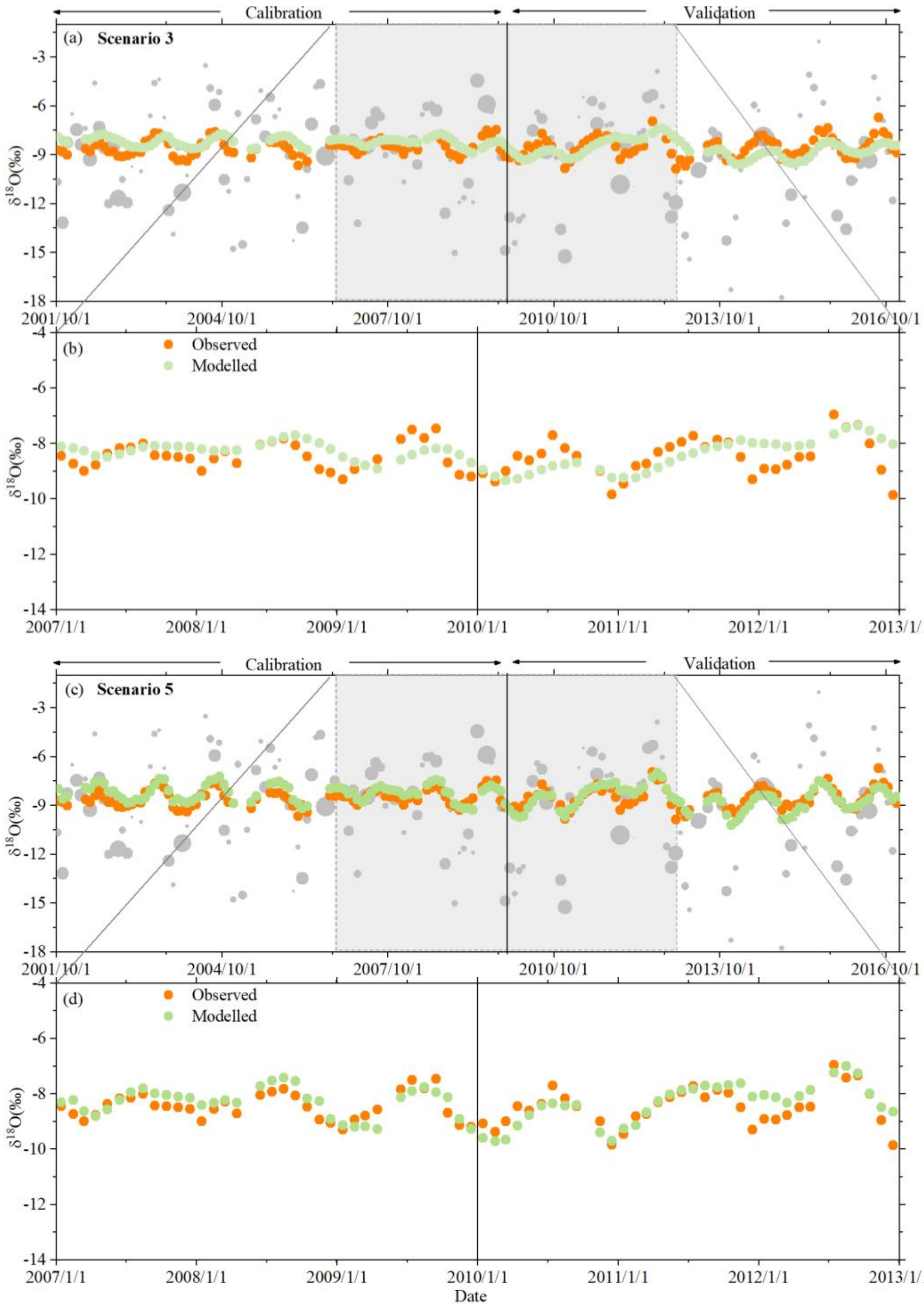

Figure S6. The time series of stream δ^{18}O reproduced by CO models, i.e., calibration strategy $C_{\delta^{18}O}$ (scenario3, 5), for the model calibration and evaluation periods. (a) Observed δ^{18}Osignals in precipitation (light grey dots; size of dots indicates the precipitation volume) and observed stream δ^{18}Osignals (orange dots) as well as the modelled stream δ^{18}Osignals (light green dots) for scenarios 3, (b) zoom-in of observed and modelled δ^{18}O signals in the stream for the 01/01/2007 – 31/12/2012 period for scenarios 3, (c) Observed δ^{18}Osignals in precipitation and in stream same as (a), and the modelled stream δ^{18}Osignals (relatively darker green dots) for scenarios 5, (d) zoom-in of observed and modelled δ^{18}O signals in the stream for the 01/01/2007 – 31/12/2012 period for scenarios 5.

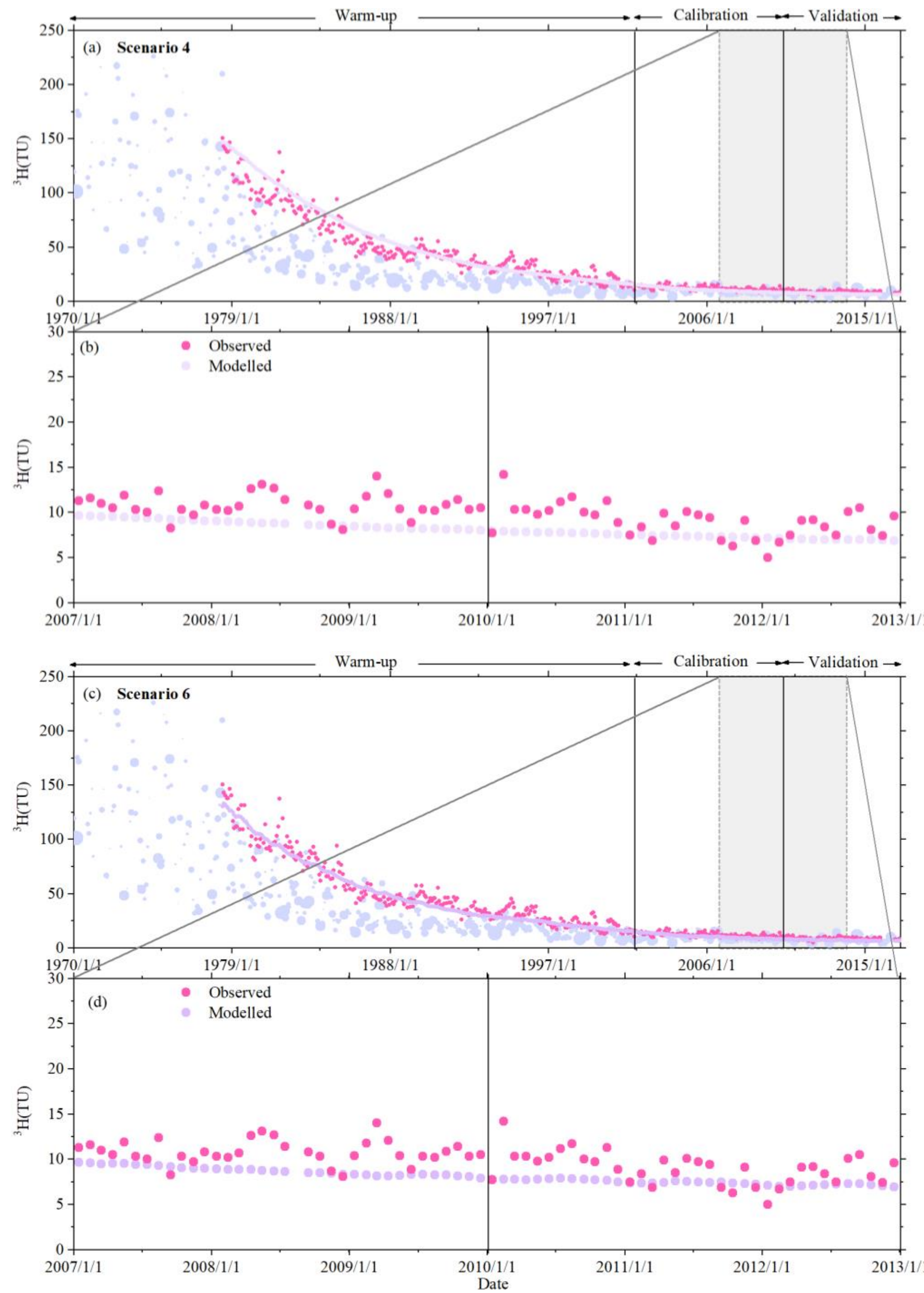

Figure S7. Time series of stream ^{3}H reproduced by CO models, i.e., calibration strategy $C_{^3H}$ (scenario4, 6), for the model calibration and evaluation periods. (a) Observed ^{3}H signals in precipitation (light blue-purple dots; size of dots indicates associated precipitation volume) and in streamflow (pink dots) as well as the modelled ^{3}H stream signal (light purple dots), (b) zoom-in of observed and modelled ^{3}H signals for the 01/01/2007 – 31/12/2012 period for scenarios 4, (c) Observed ^{3}H signals in precipitation and in stream same as (a), and the modelled stream ^{3}H signals (relatively darker purple dots) for scenarios 6, (d) zoom-in of observed and modelled ^{3}H signals in the stream for the 01/01/2007 – 31/12/2012 period for scenarios 6.

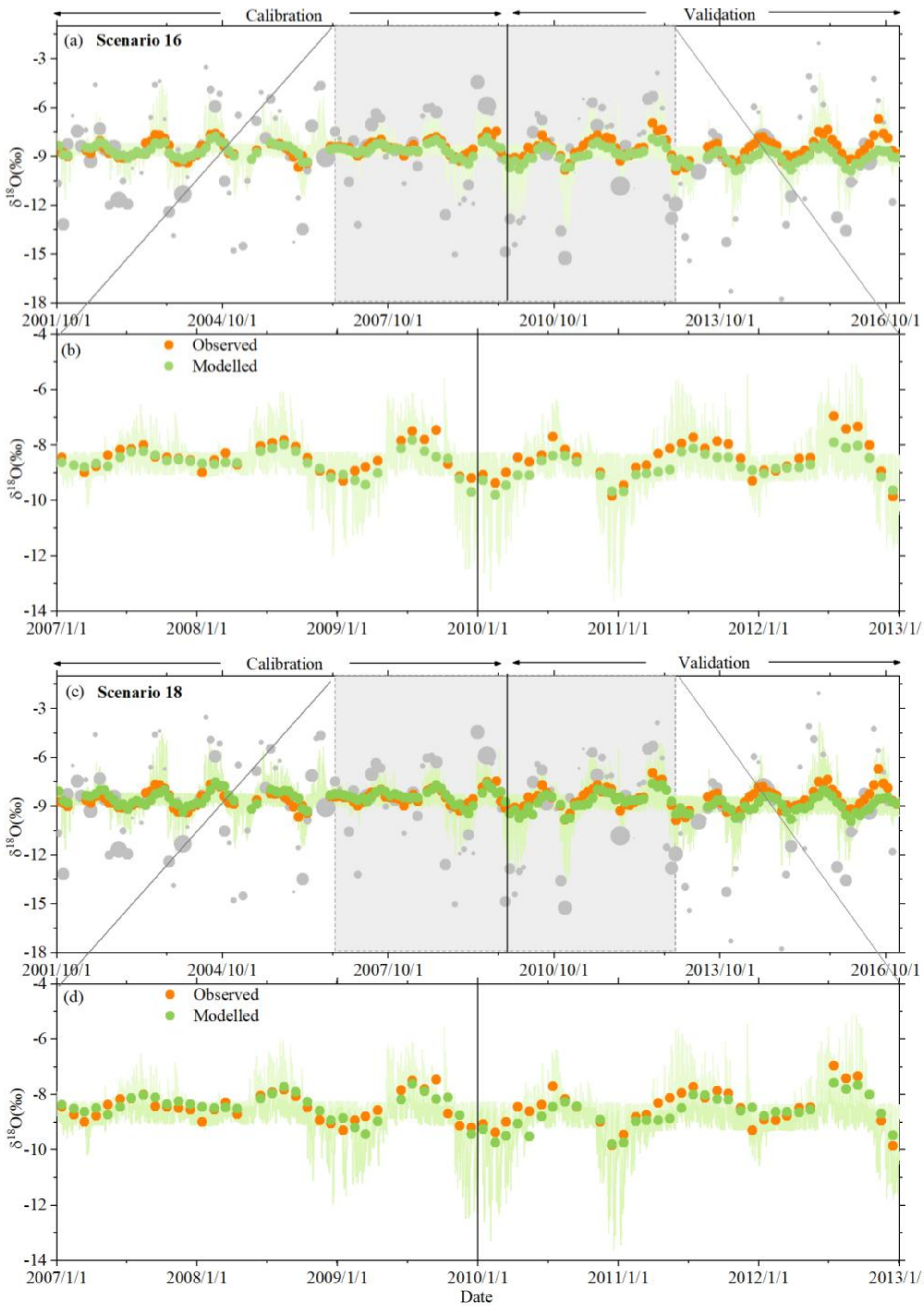

Figure S8. The time series of stream $\delta^{18}O$ reproduced by IM-SAS-L models based on simultaneous calibration to $\delta^{18}O$ and the streamflow signatures, i.e., calibration strategy $C_{\delta^{18}O,Q}$ (scenario 16) and $C_{\delta^{18}O,^{3}H,Q}$ (scenario 18), for the model calibration and evaluation periods. (a) Observed $\delta^{18}O$signals in precipitation (light grey dots; size of dots indicates the precipitation volume) and observed stream $\delta^{18}O$signals (orange dots) as well as the modelled stream $\delta^{18}O$signals (green dots) and the 5th/95th percentile of all retained pareto optimal solutions obtained from calibration strategy $C_{\delta^{18}O,Q}$ (light green shaded area) for scenarios 16, (b) zoom-in of observed and modelled $\delta^{18}O$ signals in the stream for the 01/01/2007 – 31 /12/2012 period for scenarios 16, (c) Observed $\delta^{18}O$signals in precipitation and in stream same as (a), and the modelled stream δ^{18}Osignals (relatively darker green dots) with the 5th/95th percentile of all retained pareto optimal solutions obtained from calibration strategy $C_{\delta^{18}O,{}^{3}H,Q}$ (light green shaded area) for scenarios 18, (d) zoom-in of observed and modelled δ^{18}O signals in the stream for the 01/01/2007 – 31/12/2012 period for scenarios 18.

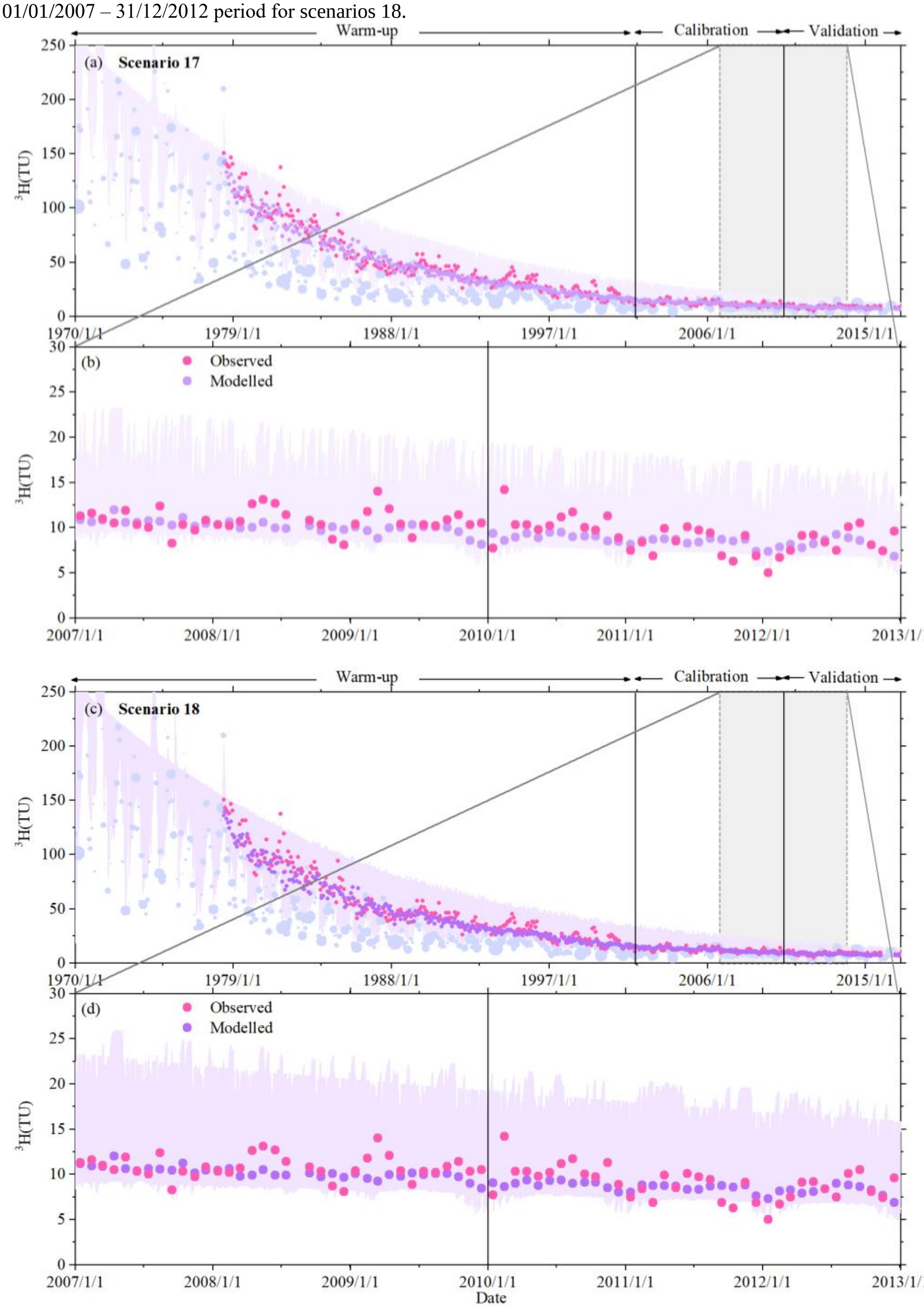

Figure S9. Time series of stream ^{3}H reproduced by model IM-SAS-L based on simultaneous calibration to tracer and the streamflow signatures, i.e. calibration strategy $C_{{}^{3}H,Q}$ (scenario 17) and $C_{\delta^{18}O,{}^{3}H,Q}$ (scenario 18), for the model calibration and evaluation periods. (a) Observed ^{3}H signals in precipitation (light blue-purple dots; size of dots indicates associated precipitation volume) and in streamflow (pink dots) as well as the modelled ^{3}H stream signal based on the most balanced solution, i.e. lowest DE (light purple dots), and the 5th/95th inter-quantile range of all retained pareto optimal solutions obtained from calibration strategy $C^{3}_{H,Q}$ (light purple shaded area) for scenario 17, (b) zoom-in of observed and modelled ^{3}H signals for the 01/01/2007 – 31/12/2012 period for scenario

17, (c) Observed ^{3}H signals in precipitation and in stream same as (a), and the modelled stream ^{3}H signals (relatively darker purple dots) and the $5^{th}/95^{th}$ percentile of all retained pareto optimal solutions obtained from calibration strategy $C_{\delta^{18}O,^{3}H,Q}$ (light purple shaded area) for scenarios 18, (d) zoom-in of observed and modelled ^{3}H signals in the stream for the 01/01/2007 – 31/12/2012 period for scenarios 18.

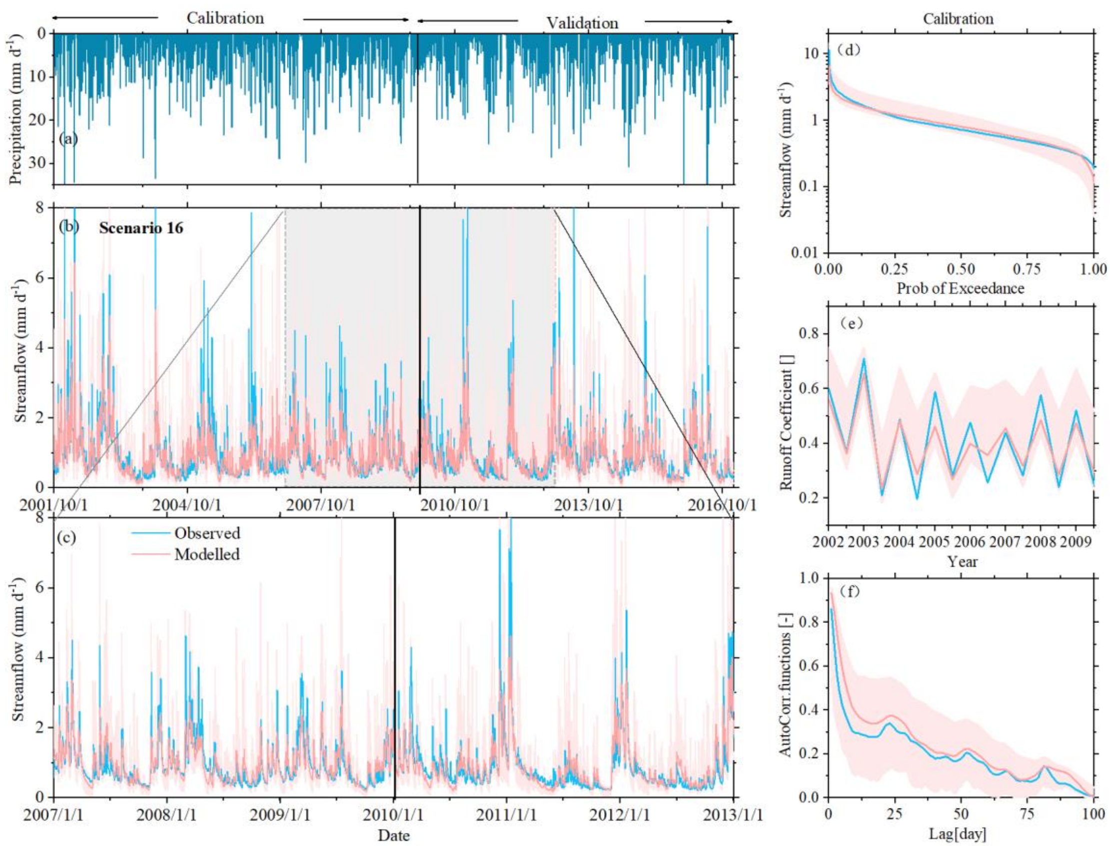

Figure S10. Hydrograph and selected hydrological signatures reproduced by IM-SAS-L, following a simultaneous calibration to the hydrological response and $\delta^{18}O$ ($C_{\delta^{18}O,Q}$; scenario 16). (a) Time series of observed daily precipitation; observed and modelled (b) daily stream flow (Q), where the light red line indicates the most balanced solution, i.e., lowest D_E, and the light red shaded area the $5^{th}/95^{th}$ inter-quantile range obtained from all pareto optimal solutions; (c) stream flow zoomed-in to the 01/01/2007 – 31/12/2012 period; (d) flow duration curves (FDC), (e) seasonal runoff coefficients (RC_Q) and (f) autocorrelation functions of stream flow (AC_Q) for the calibration period. Blue lines indicate values based on observed streamflow (Q_o), light red lines are values based on modelled stream flow (Q_m) representing the most balanced solutions, i.e., lowest D_E and the light red shaded areas show the $5^{th}/95^{th}$ inter-quantile ranges obtained from all pareto optimal solutions.

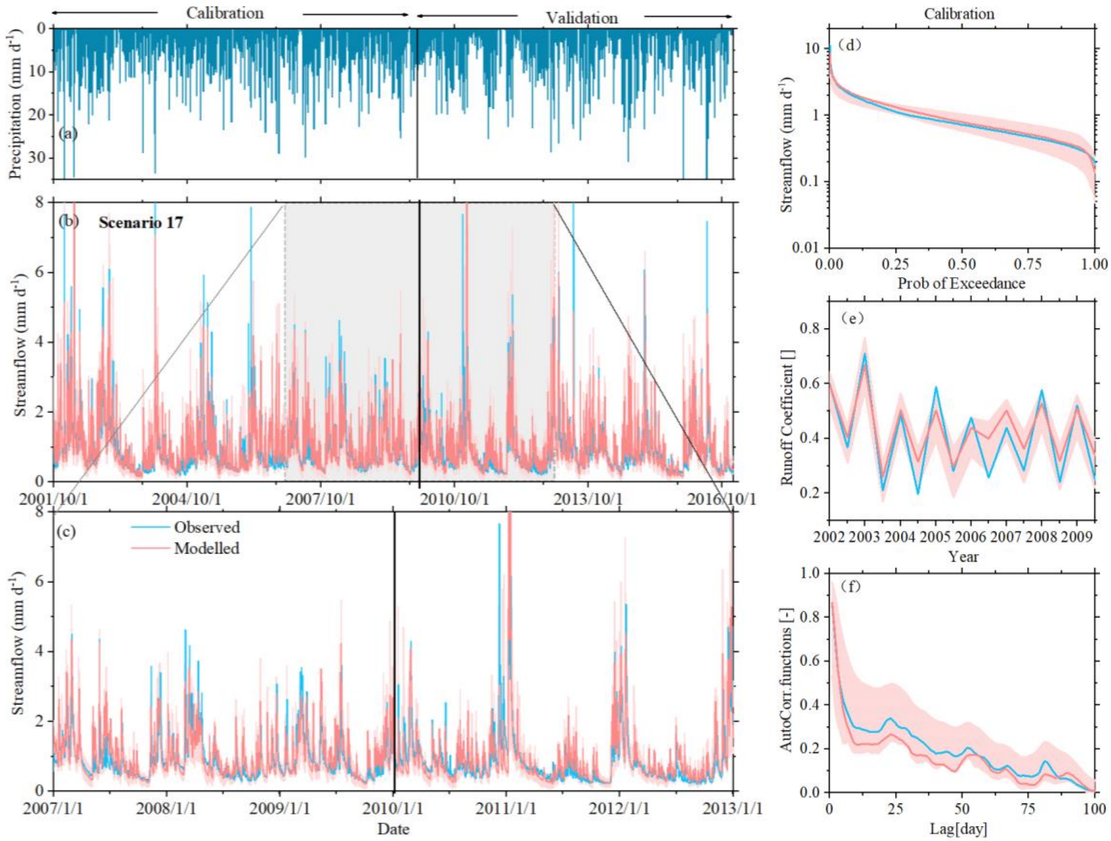

Figure S11. Hydrograph and selected hydrological signatures reproduced by IM-SAS-L, following a simultaneous calibration to the hydrological response and ^{3}H ($C_{^3H,Q}$; scenario 17). (a) Time series of observed daily precipitation; observed and modelled (b) daily stream flow (Q), where the light red line indicates the most balanced solution, i.e., lowest D_E, and the light red shaded area the $5^{th}/95^{th}$ inter-quantile range obtained from all pareto optimal solutions; (c) stream flow zoomed-in to the 01/01/2007 – 31/12/2012 period; (d) flow duration curves (FDC), (e) seasonal runoff coefficients (RC_Q) and (f) autocorrelation functions of stream flow (AC_Q) for the calibration period. Blue lines indicate values based on observed streamflow (Q_o), light red lines are values based on modelled stream flow (Q_m) representing the most balanced solutions, i.e., lowest D_E and the light red shaded areas show the $5^{th}/95^{th}$ inter-quantile ranges obtained from all pareto optimal solutions.

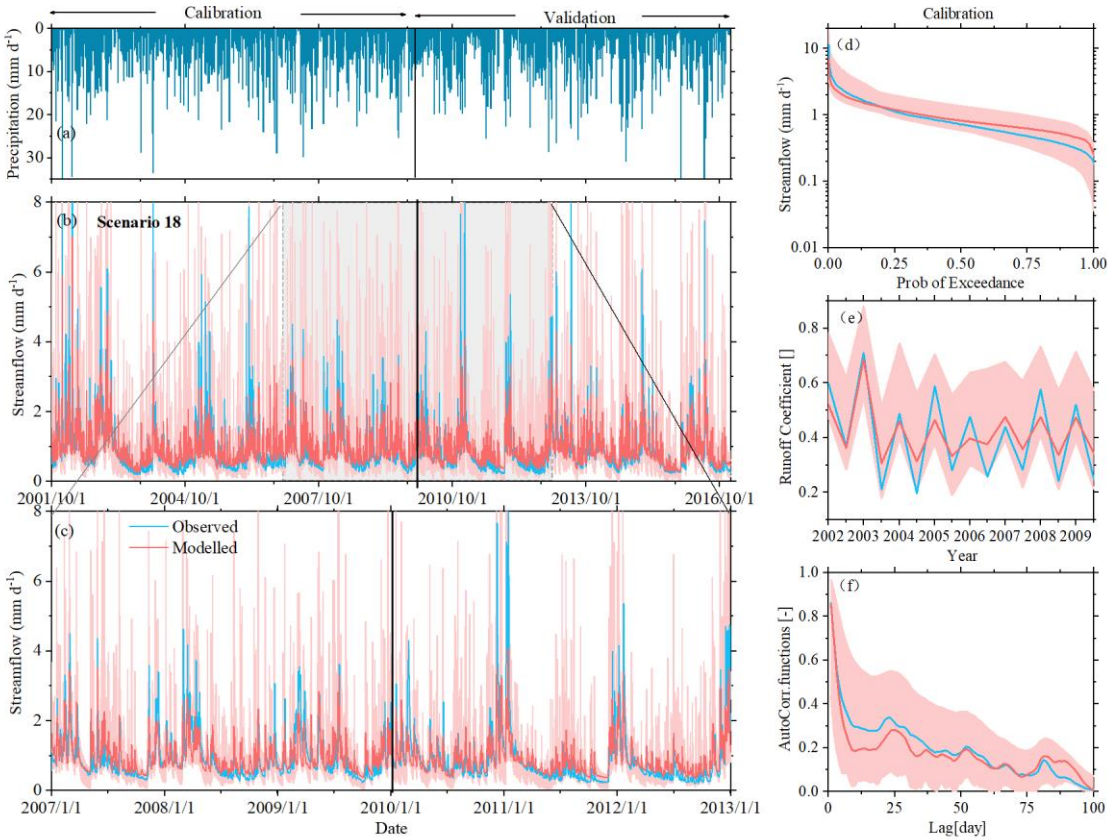

Figure S12. Hydrograph and selected hydrological signatures reproduced by IM-SAS-L, following a simultaneous calibration to the hydrological response, δ^{18}O and ^{3}H ($C_{\delta^{18}O,^{3}H,Q}$; scenario 18). (a) Time series of observed daily precipitation; observed and modelled (b) daily stream flow (Q), where the light red line indicates the most balanced solution, i.e., lowest D_E, and the light red shaded area the 5th/95th inter-quantile range obtained from all pareto optimal solutions; (c) stream flow zoomed-in to the 01/01/2007 – 31/12/2012 period; (d) flow duration curves (FDC), (e) seasonal runoff coefficients (RC_Q) and (f) autocorrelation functions of stream flow (AC_Q) for the calibration period. Blue lines indicate values based on observed streamflow (Q_o), light red lines are values based on modelled stream flow (Q_m) representing the most balanced solutions, i.e., lowest D_E and the light red shaded areas show the 5th/95th inter-quantile ranges obtained from all pareto optimal solutions.

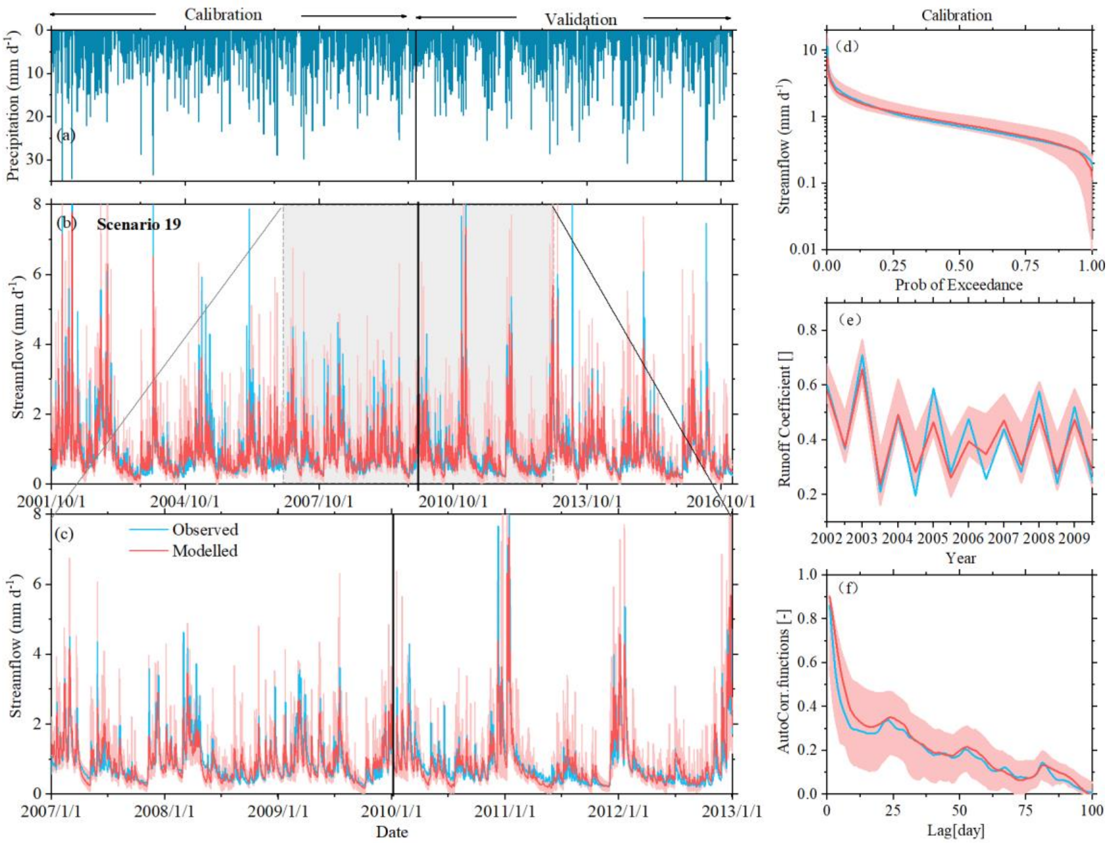

Figure S13. Hydrograph and selected hydrological signatures reproduced by IM-SAS-D, following a simultaneous calibration to the hydrological response and δ^{18}O ($C_{\delta^{18}O,Q}$; scenario 19). (a) Time series of observed daily precipitation; observed and modelled (b) daily stream flow (Q), where the light red line indicates the most balanced solution, i.e., lowest D_E, and the light red shaded area the $5^{th}/95^{th}$ inter-quantile range obtained from all pareto optimal solutions; (c) stream flow zoomed-in to the 01/01/2007 – 31/12/2012 period; (d) flow duration curves (FDC), (e) seasonal runoff coefficients (RC_Q) and (f) autocorrelation functions of stream flow (AC_Q) for the calibration period. Blue lines indicate values based on observed streamflow (Q_o), light red lines are values based on modelled stream flow (Q_m) representing the most balanced solutions, i.e., lowest D_E and the light red shaded areas show the $5^{th}/95^{th}$ inter-quantile ranges obtained from all pareto optimal solutions.

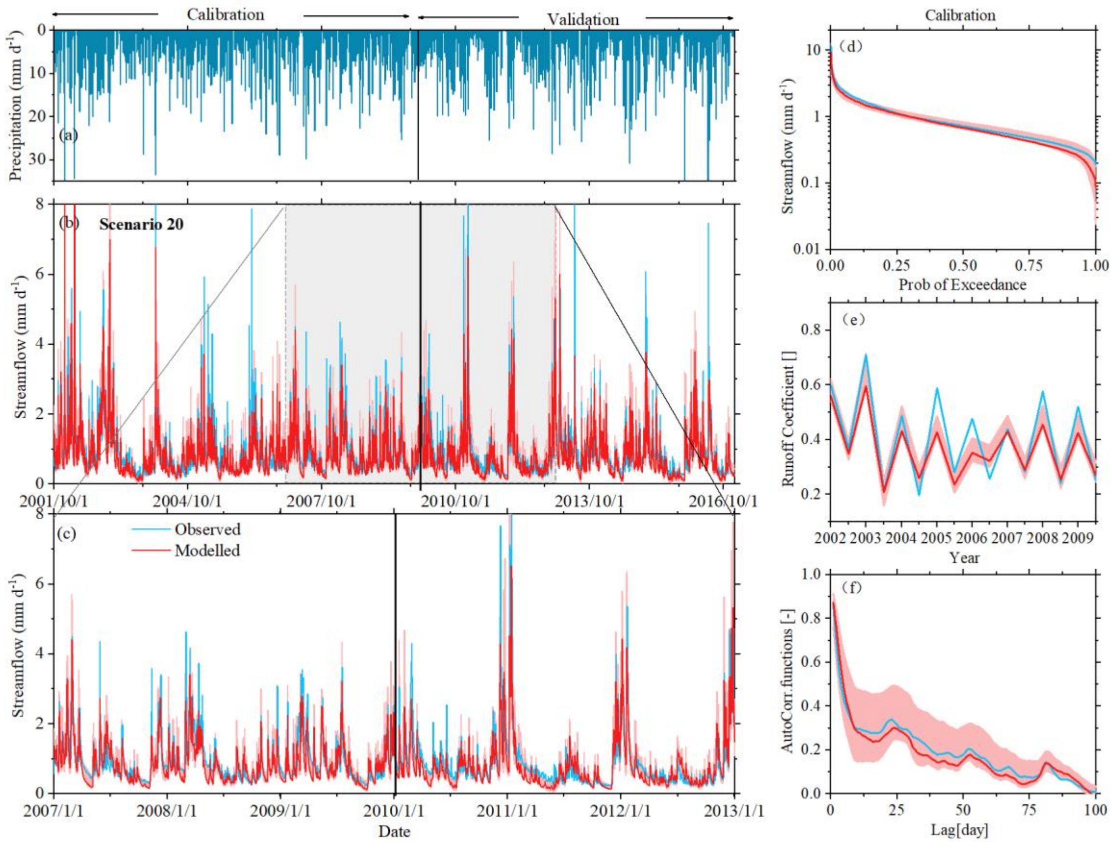

Figure S14. Hydrograph and selected hydrological signatures reproduced by IM-SAS-D, following a simultaneous calibration to the hydrological response and ^{3}H ($C_{^3H,Q}$; scenario 20). (a) Time series of observed daily precipitation; observed and modelled (b) daily stream flow (Q), where the red line indicates the most balanced solution, i.e., lowest D_E, and the light red shaded area the 5th/95th inter-quantile range obtained from all pareto optimal solutions; (c) stream flow zoomed-in to the 01/01/2007 – 31/12/2012 period; (d) flow duration curves (FDC), (e) seasonal runoff coefficients (RC_Q) and (f) autocorrelation functions of stream flow (AC_Q) for the calibration period. Blue lines indicate values based on observed streamflow (Q_o), red lines are values based on modelled stream flow (Q_m) representing the most balanced solutions, i.e., lowest D_E and the light red shaded areas show the 5th/95th inter-quantile ranges obtained from all pareto optimal solutions.

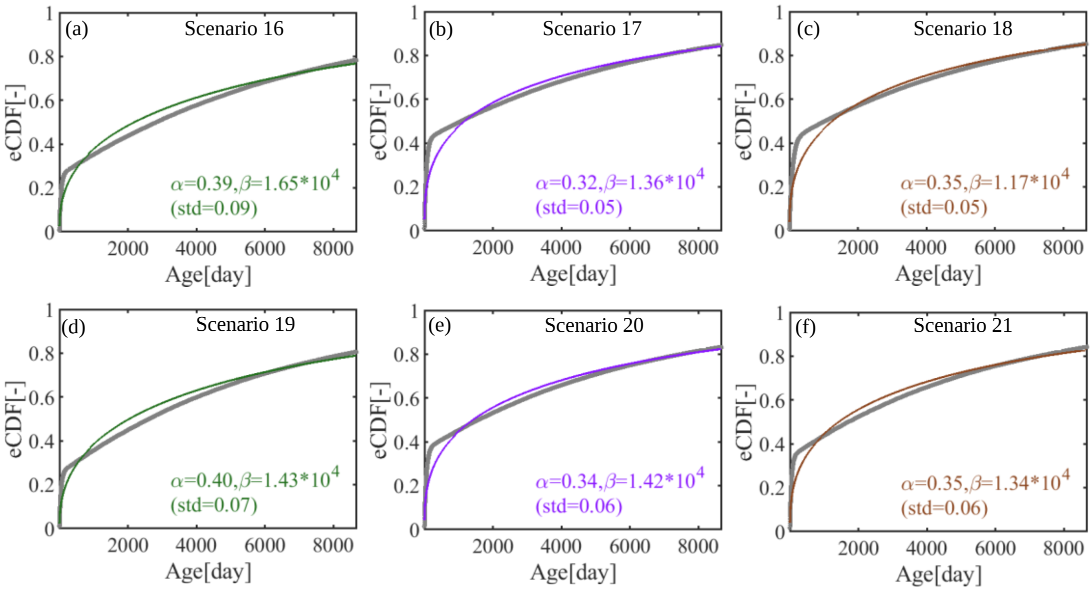

Figure S15. The Gamma distributions to the volume-weighted mean steam flow TTDs of model IM-SAS (i.e., scenarios 16-21) based on model IM-SAS-L in (a)-(c) and model IM-SAS-D in (d)-(f). Grey shades in (a)-(f) indicate volume-weighted mean TTDs and colored shades indicate the corresponding fitting Gamma distributions, respectively.

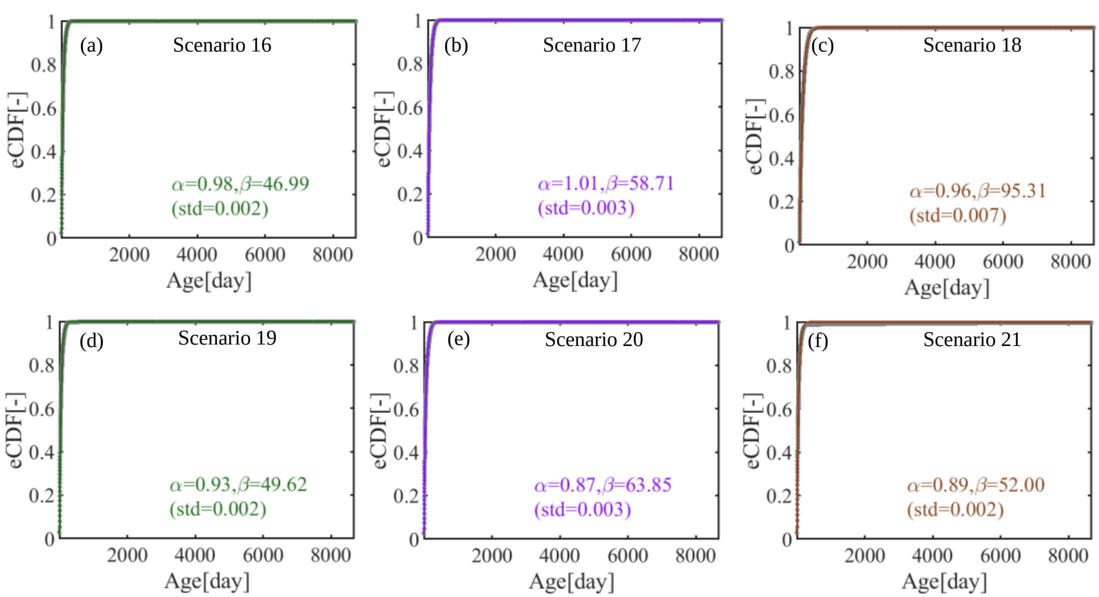

Figure S16. The Gamma distributions to the volume-weighted mean transpiration (E_a) TTDs of model IM-SAS (i.e., scenarios 16-21) based on model IM-SAS-L in (a)-(c) and model IM-SAS-D in (d)-(f). Grey shades in (a)-(f) indicate volume-weighted mean TTDs and colored shades indicate the corresponding fitting Gamma distributions, respectively.

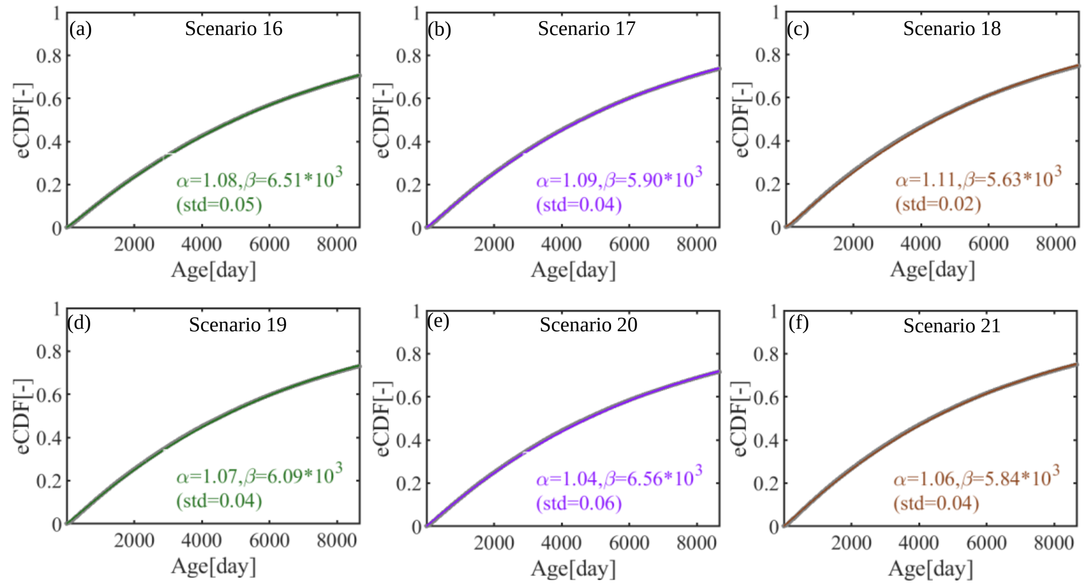

Figure S17. The Gamma distributions to the volume-weighted mean groundwater (S_s) RTDs of model IM-SAS (i.e., scenarios 16-21) based on model IM-SAS-L in (a)-(c) and model IM-SAS-D in (d)-(f). Grey shades in (a)-(f) indicate volume-weighted mean RTDs and colored shades indicate the corresponding fitting Gamma distributions, respectively.

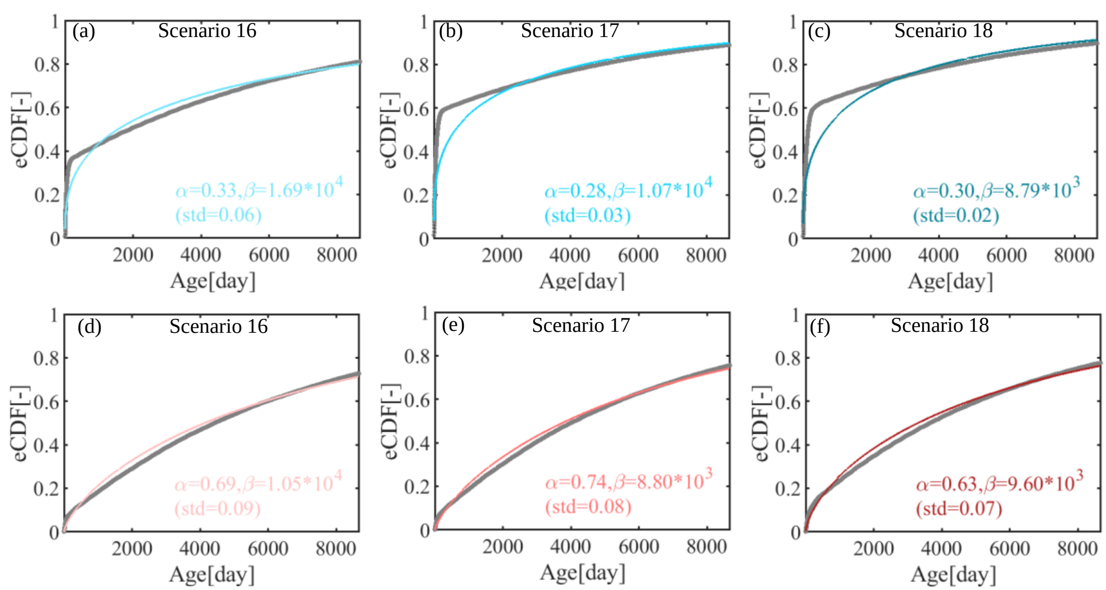

Figure S18. The Gamma distributions to the volume-weighted mean steam flow TTDs for the wet and dry periods of model IM-SAS-L (i.e., scenarios 16-18) based on wet periods in (a)-(c) and dry periods in (d)-(f). Grey shade and blue shades in (a)-(c) indicate volume-weighted mean TTDs for wet periods and the corresponding fitting Gamma distributions, respectively; grey shade and red shades in (d)-(f) indicate volume-weighted mean TTDs for dry periods and the corresponding fitting Gamma distributions, respectively.

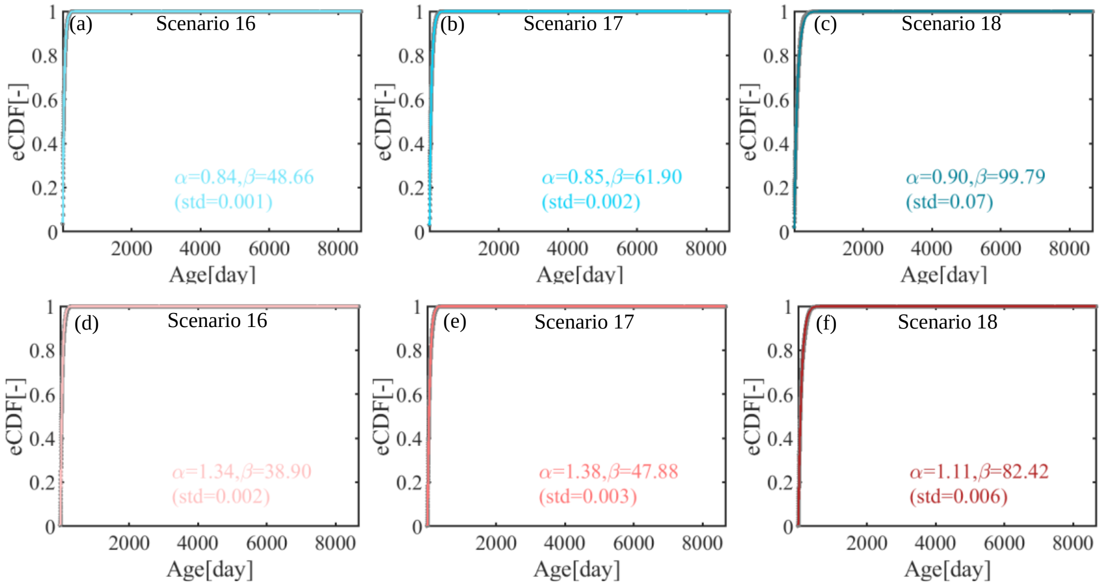

Figure S19. The Gamma distributions to the volume-weighted mean transpiration (E_a) TTDs for the wet and dry periods of model IM-SAS-L (i.e., scenarios 16-18) based on wet periods in (a)-(c) and dry periods in (d)-(f). Grey shade and blue shades in (a)-(c) indicate volume-weighted mean TTDs for wet periods and the corresponding fitting Gamma distributions, respectively; grey shade and red shades in (d)-(f) indicate volume-weighted mean TTDs for dry periods and the corresponding fitting Gamma distributions, respectively.

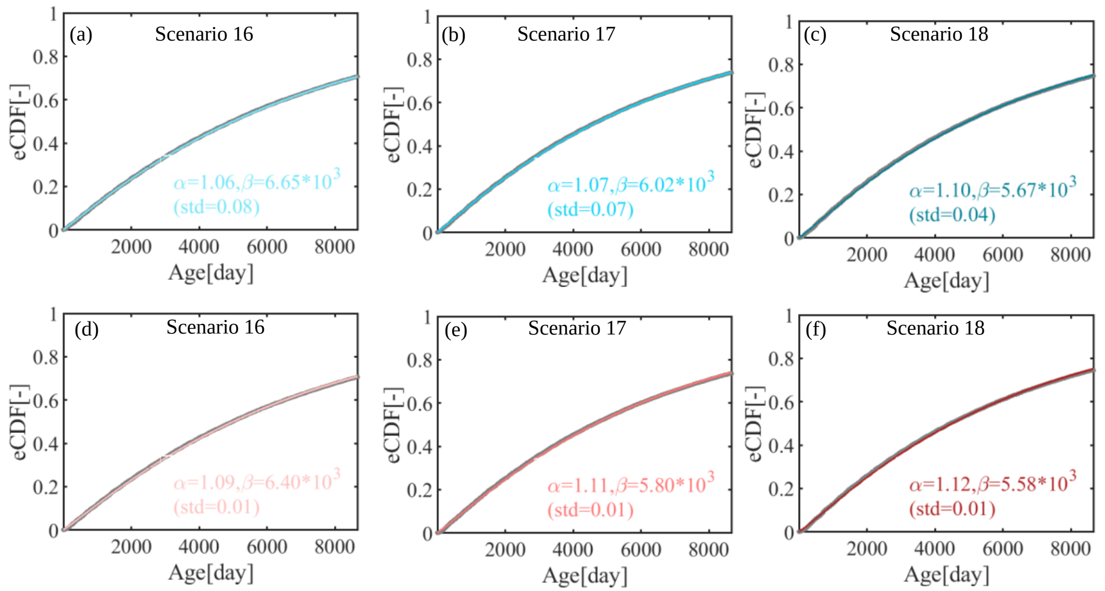

Figure S20. The Gamma distributions to the volume-weighted mean groundwater (S_s) RTDs for the wet and dry periods of model IM-SAS-L (i.e., scenarios 16-18) based on wet periods in (a)-(c) and dry periods in (d)-(f). Grey shade and blue shades in (a)-(c) indicate volume-weighted mean RTDs for wet periods and the corresponding fitting Gamma distributions, respectively; grey shade and red shades in (d)-(f) indicate volume-weighted mean RTDs for dry periods and the corresponding fitting Gamma distributions, respectively.

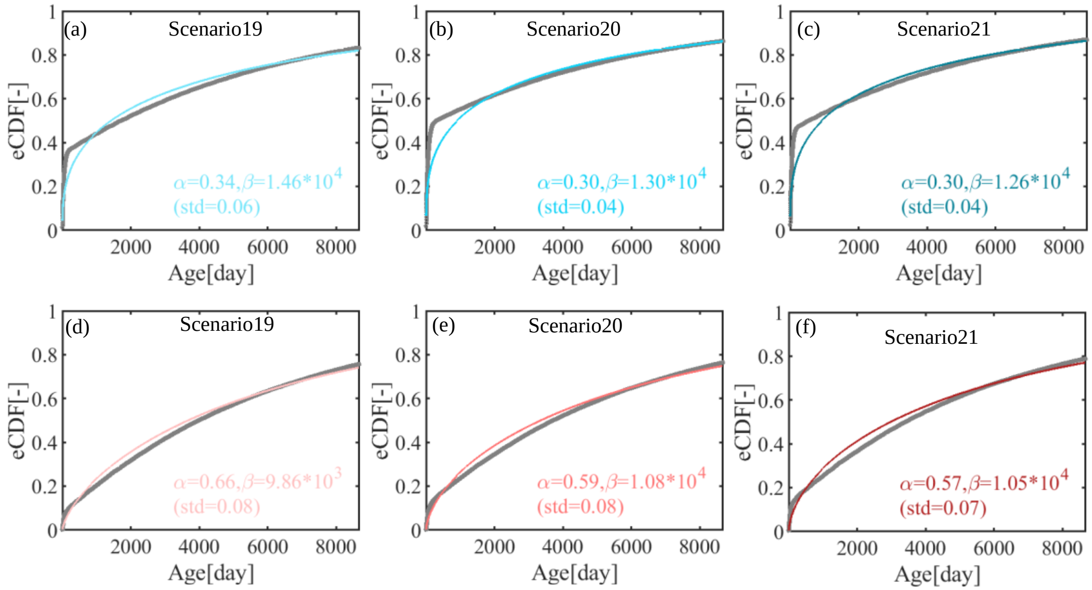

Figure S21. The Gamma distributions to the volume-weighted mean steam flow TTDs for the wet and dry periods of model IM-SAS-D (i.e., scenarios 19-21) based on wet periods in (a)-(c) and dry periods in (d)-(f). Grey shade and blue shades in (a)-(c) indicate volume-weighted mean TTDs for wet periods and the corresponding fitting Gamma distributions, respectively; grey shade and red shades in (d)-(f) indicate volume-weighted mean TTDs for dry periods and the corresponding fitting Gamma distributions, respectively.

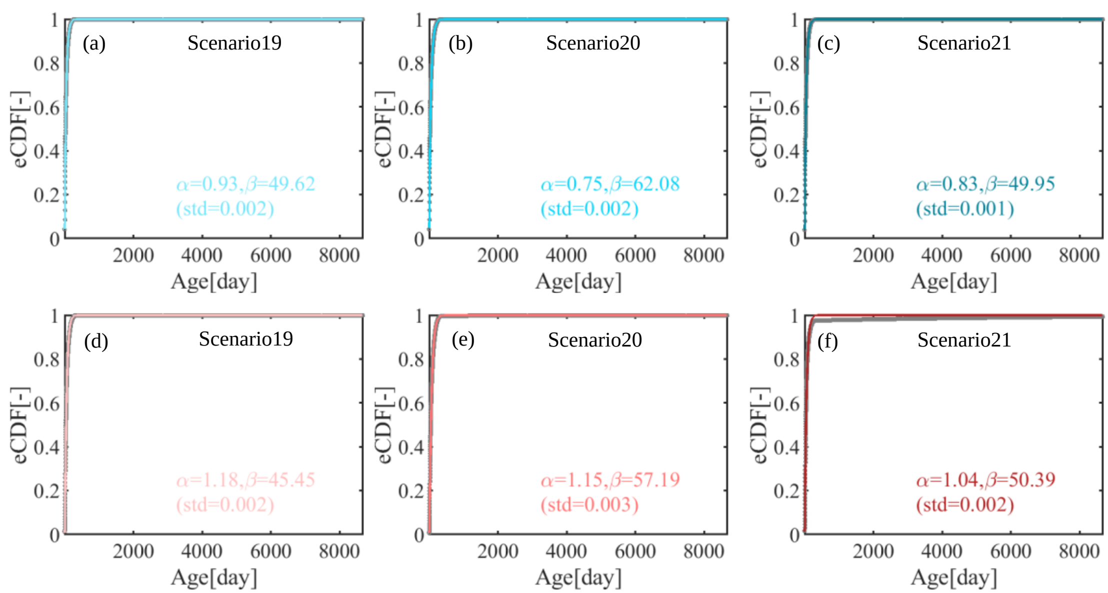

Figure S22. The Gamma distributions to the volume-weighted mean transpiration (E_a) TTDs for the wet and dry periods of model IM-SAS-D (i.e., scenarios 19-21) based on wet periods in (a)-(c) and dry periods in (d)-(f). Grey shade and blue shades in (a)-(c) indicate volume-weighted mean TTDs for wet periods and the corresponding fitting Gamma distributions, respectively; grey shade and red shades in (d)-(f) indicate volume-weighted mean TTDs for dry periods and the corresponding fitting Gamma distributions, respectively.

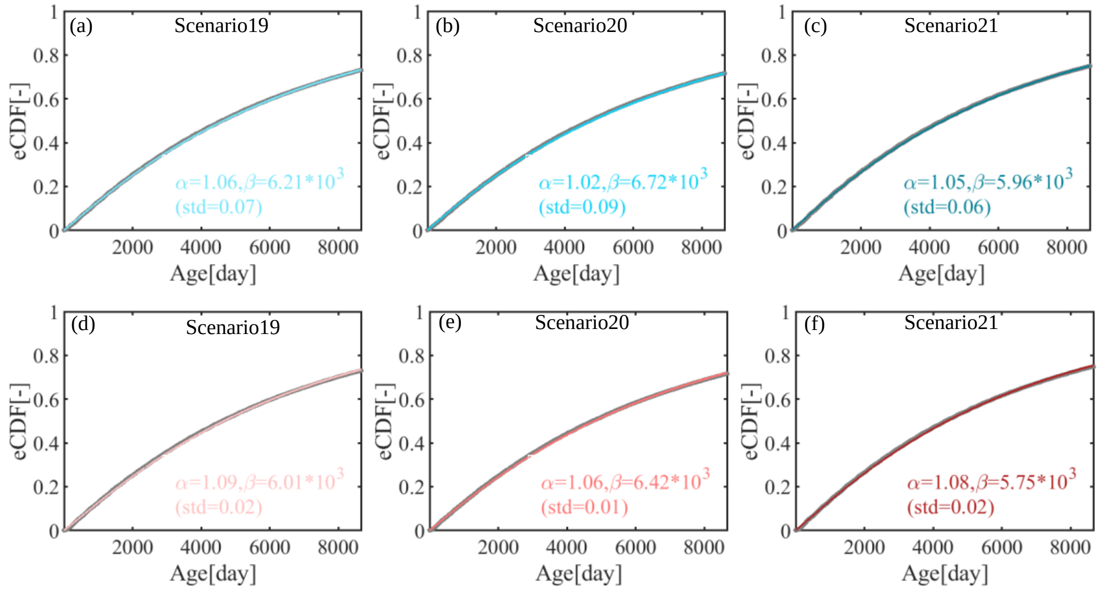

Figure S23. The Gamma distributions to the volume-weighted mean groundwater (S_s) RTDs for the wet and dry periods of model IM-SAS-D (i.e., scenarios 19-21) based on wet periods in (a)-(c) and dry periods in (d)-(f). Grey shade and blue shades in (a)-(c) indicate volume-weighted mean RTDs for wet periods and the corresponding fitting Gamma distributions, respectively; grey shade and red shades in (d)-(f) indicate volume-weighted mean RTDs for dry periods and the corresponding fitting Gamma distributions, respectively.

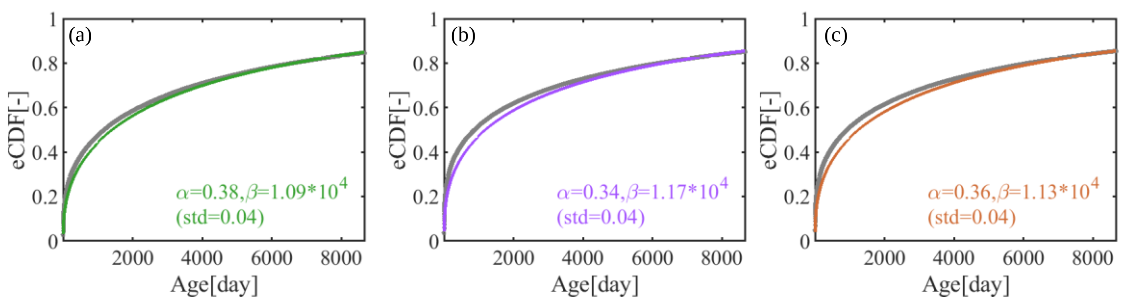

Figure S24. The Gamma distributions to the volume-weighted mean steam flow TTDs (i.e., scenarios 13-15). Grey shades in (a)-(c) indicate volume-weighted mean TTDs and colored shades indicate the corresponding fitting Gamma distributions (green for Scenario 13, purple for scenario 14 and brown for scenario 15), respectively.

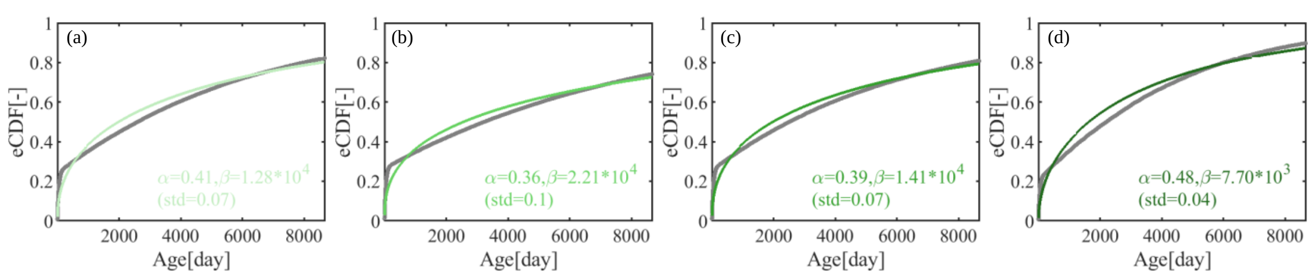

Figure S25. The Gamma distributions to the volume-weighted mean steam flow TTDs of each precipitation zone based on model IM-SAS-D from scenario 19. Grey shades in (a)-(d) indicate volume-weighted mean TTDs of four precipitation zones (P1-P4) and colored shades indicate the corresponding fitting Gamma distributions, respectively.

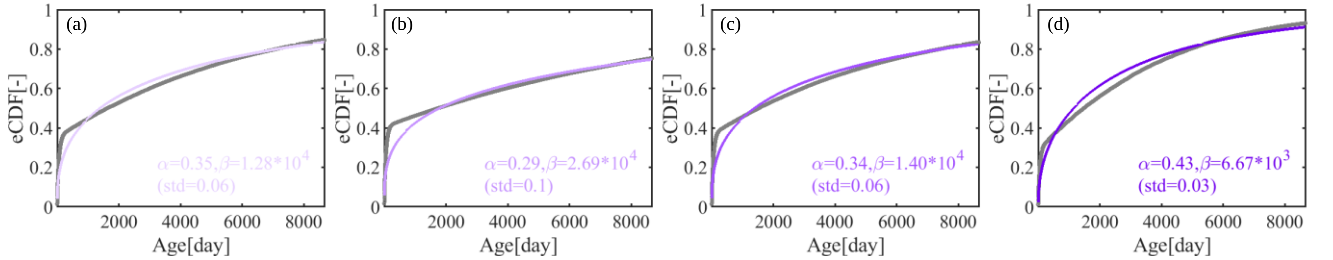

Figure S26. The Gamma distributions to the volume-weighted mean steam flow TTDs of each precipitation zone based on model IM-SAS-D from scenario 20. Grey shades in (a)-(d) indicate volume-weighted mean TTDs of four precipitation zones (P1-P4) and colored shades indicate the corresponding fitting Gamma distributions, respectively.

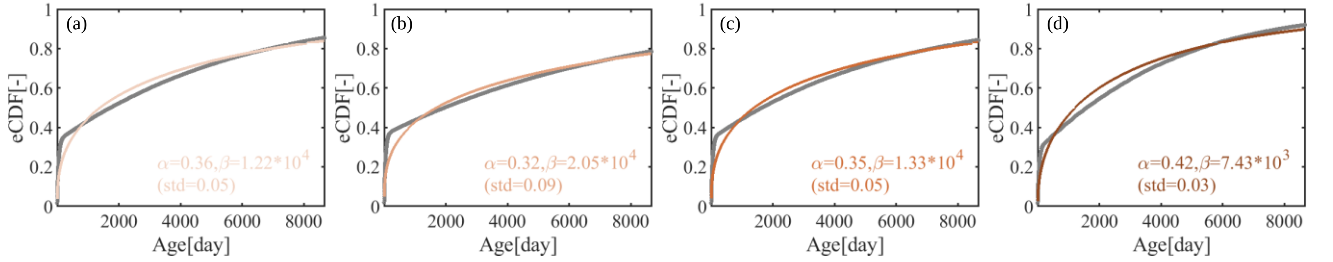

Figure S27. The Gamma distributions to the volume-weighted mean steam flow TTDs of each precipitation zone based on model IM-SAS-D from scenario 21. Grey shades in (a)-(d) indicate volume-weighted mean TTDs of four precipitation zones (P1-P4) and colored shades indicate the corresponding fitting Gamma distributions, respectively.

Table S3. Water balance and constitutive equations of distributed hydrological model

Reservoirs	Water balance		Constitutive equations	
Interception	$\frac{ds_i}{dt} = P_{rain} - E_i - P_{re}$	(S4)	$P_{rain} = P, when\ T > T_t$	(S10)
			$E_i = \min(E_p, S_i/dt)$	(S11)
			$P_{re} = \max((S_i - S_{imax})/dt, 0)$	(S12)
Snow	$\frac{ds_{snow}}{dt} = P_{snow} - M_{snow}$	(S5)	$P_{snow,e} = P, when\ T_e \leq T_t$	(S13)
			$P_{snow} = \sum P_{snow,e} \cdot W_e$	(S14)
			$M_{snow,e} = \min(C_{melt} * (T_e - T_t), S_{snow,e}/dt), when\ T_e > T_t$	(S15)
			$M_{snow} = \sum M_{snow,e} \cdot W_e$	(S16)
Unsaturated reservoir	Forest/ Grass: $\frac{ds_u}{dt} = P_e - E_a - R_u - R_{perc}$	(S6)	$P_e = P_{re} + M_{snow}$	(S17)
			$\rho = S_u/S_{umax}$	(S18)
			$E_a = (E_p - E_i) * \min(\rho/C_a, 1)$	(S19)
			$C_r = 1 - (1-\rho)^{\gamma}$	(S20)
	Wetland: $\frac{ds_u}{dt} = P_e - E_a - R_u + R_{cap}$	(S7)	$R_u = (1 - C_r) * P_e$	(S21)
			$R_{perc} = \min(c_{pmax} * \rho, S_u/dt)$	(S22)
			$R_{cap} = \min(c_{pmax} * (1-\rho), \frac{S_s}{dt} * P_{HRU})$	(S23)
			$R_{pref} = (1 - D) * R_u$	(S24)
Fast reservoir	$\frac{ds_f}{dt} = R_f - Q_f$	(S8)	Forest/ Grass: $R_f = D * R_u$	(S25)
			Wetland: $R_f = R_u$	(S26)
			$Q_f = K_f * S_f$	(S27)
Slow reservoir	$\frac{ds_s}{dt} = R_{perctot} + R_{preftot} - R_{captot} - Q_s$	(S9)	$R_{perctot} = \sum R_{perc} \cdot P_{HRU}$	(S28)
			$R_{preftot} = \sum R_{pref} \cdot P_{HRU}$	(S29)
			$R_{captot} = \sum R_{cap} \cdot P_{HRU}$	(S30)
			$Q_s = K_s * S_s$	(S31)

Table S4. Model parameters and their constraints in Borg_MOEA method.

	Parameters	Unit	Description	Parameter Constraints	References
Global	T_t	°C	Threshold temperature to split snowfall and rainfall		(Gao et al., 2014; Hrachowitz et al., 2013)
	C_{melt}	mm °C^{-1}	Melt factor		(Prenner et al., 2018)
	C_a	-	Evapotranspiration coefficient		(Gao et al., 2017)
	K_s	d^{-1}	Recession coefficient of slow response reservoir		(Prenner et al., 2018)
	Ssp	mm	Passive storage Volume		(Hrachowitz et al., 2021)
Forest	S_{imaxF}	mm	Interception capacity	S_{imaxF}>S_{imaxG}	(Gao et al., 2014)
	S_{umaxF}	mm	Root zone storage capacity	S_{umaxF}>S_{umaxG}	(Gao et al., 2014)
	γ_F	-	Shape parameter		(Gao et al., 2014)
	D	-	Splitter to fast and slow response reservoirs		(Gao et al., 2014)
	c_{pmaxF}	mm d^{-1}	Percolation capacity		(Prenner et al., 2018)
	K_{fF}	d^{-1}	Recession coefficient of fast response reservoir	K_{fF}>K_s	(Hrachowitz et al., 2013)
Grassland	S_{imaxG}	mm	Interception capacity		(Gao et al., 2014)
	S_{umaxG}	mm	Root zone storage capacity	S_{umaxG}>S_{umaxW}	(Gao et al., 2014)
	γ_G	-	Shape parameter		(Gao et al., 2014)
	c_{pmaxG}	mm d^{-1}	Percolation capacity		(Prenner et al., 2018)
	K_{fG}	d^{-1}	Recession coefficient of fast response reservoir	K_{fG}>K_s	(Hrachowitz et al., 2013)
Wetland	S_{umaxW}	mm	Root zone storage capacity	$S_{umaxW} < S_{umaxG}$	(Gao et al., 2014)
	γ_W	-	Shape parameter		(Gao et al., 2014)
	c_{rmax}	mm d^{-1}	Percolation capacity		(Gao et al., 2014)
	K_{fW}	d^{-1}	Recession coefficient of fast response reservoir	K_{fW}>K_s	(Prenner et al., 2018)

Table S5. Performance metrics of the model implementations and the associated calibration strategies for the 2001 – 2009 calibration period (cal.) and the 2010 – 2016 model evaluation period (val.). The ranges of all performance metrics for the full set of pareto optimal solutions for the multi-objective calibration cases (Scenarios 15 – 21) are shown here.

	Scenario		15	16	17	18	19	20	21
	Model		P-SAS		IM-SAS-L			IM-SAS-D	
	Implementation				Lumped			Distributed	
	Calibration strategy → Performance metric ↓		$C_{\delta^{18}O,^3H}$	$C_{\delta^{18}O,Q}$	$C_{^3H,Q}$	$C_{\delta^{18}O,^3H,Q}$	$C_{\delta^{18}O,Q}$	$C_{^3H,Q}$	$C_{\delta^{18}O,^3H,Q}$
Performance metrics	$MSE_{\delta^{18}O}$	cal.	0.069-0.080	0.070-0.347	-	0.068-0.756	0.068-0.188	-	0.068-0.262
		val.	0.212-0.216	0.134-0.733	-	0.116-1.006	0.129-0.648	-	0.141-0.905
	$MSE_{^3H}$	cal.	2.846-2.869	-	2.972-71.69	2.823-130.6	-	2.956-19.75	2.975-47.54
		val.	1.704-1.758	-	1.825-19.97	1.908-40.46	-	1.932-4.883	1.915-13.29
	MSE_Q	cal.	-	0.194-1.287	0.193-0.703	0.196-2.762	0.228-0.817	0.232-0.442	0.248-1.161
		val.	-	0.211-1.239	0.212-0.706	0.215-2.572	0.251-0.827	0.253-0.454	0.273-1.118
	$MSE_{log(Q)}$	cal.	-	0.090-0.584	0.091-0.304	0.098-0.621	0.119-0.334	0.101-0.231	0.112-0.399
		val.	-	0.088-0.662	0.080-0.362	0.083-0.582	0.101-0.321	0.088-0.310	0.105-0.485
	MSE_{FDC_Q}	cal.	-	0.003-0.359	0.003-0.129	0.003-1.042	0.002-0.144	0.002-0.072	0.002-0.212
		val.	-	0.004-0.369	0.002-0.195	0.007-0.877	0.003-0.141	0.012-0.111	0.004-0.180
	$MSE_{FDC_{log(Q)}}$	cal.	-	0.001-0.173	0.002-0.126	0.002-0.377	0.002-0.119	0.002-0.051	0.002-0.167
		val.	-	0.003-0.229	0.002-0.207	0.003-0.345	0.002-0.093	0.004-0.127	0.003-0.251
	MSE_{RC}	cal.	-	0.003-0.045	0.003-0.011	0.003-0.070	0.003-0.018	0.002-0.006	0.002-0.026
		val.	-	0.003-0.040	0.002-0.011	0.002-0.064	0.002-0.016	0.002-0.008	0.002-0.023
	MSE_{AC_Q}	cal.	-	0.000-0.030	0.000-0.019	0.000-0.034	0.000-0.013	0.000-0.016	0.000-0.019
		val.	-	0.000-0.034	0.000-0.026	0.000-0.045	0.000-0.027	0.000-0.019	0.000-0.031

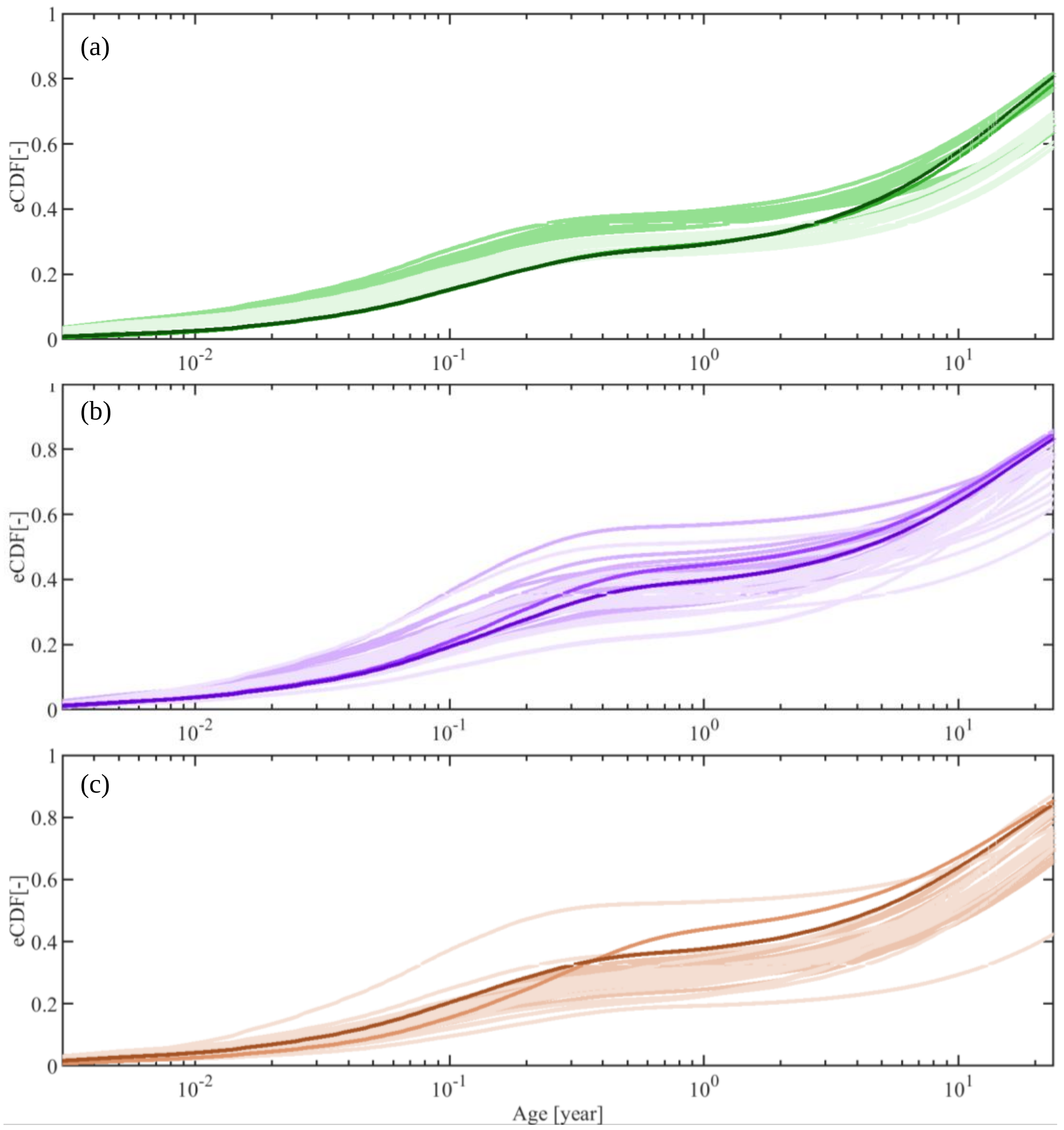

Figure S28. Stream flow TTDs derived from the 6 model scenarios based on IM-SAS models with the different associated calibration strategies (scenarios 16-21). The selected volume weighted average daily TTDs during the modelling period 01/10/2001 – 31/12/2016 are given. (a) The TTDs inferred from $\delta^{18}O$; the lightest green lines represent the TTDs based on selected solutions with scenario 16; the relatively lighter green lines represent the TTDs based on selected solutions with scenario 19; the green line represents the TTDs based on best-fit solution with scenario 16; the dark green line represents the TTDs based on best-fit solution with scenario 19; (b) The TTDs inferred from ^{3}H; the lightest purple lines represent the TTDs based on selected solutions with scenario 17; the relatively lighter purple lines represent the TTDs based on selected solutions with scenario 20; the purple line represents the TTDs based on best-fit solution with scenario 17; the dark purple line represents the TTDs based on best-fit solution with scenario 20; (c) The TTDs inferred from combined $\delta^{18}O$ and ^{3}H; the lightest brown lines represent the TTDs based on selected solutions with scenario 18; the relatively lighter brown lines represent the TTDs based on selected solutions with scenario 21; the brown line represents the TTDs based on best-fit solution with scenario 18; the dark brown line represents the TTDs based on best-fit solution with scenario 21.

Table S6. Metrics of stream flow TTDs for four precipitation zones (P1-P4) derived from the IM-SAS-D model with the different associated calibration strategies, where $C_{\delta^{18}O}$ indicates calibration to $\delta^{18}O$, $C_{^{3}H}$ calibration to ^{3}H, while $C_{\delta^{18}O,Q}$, $C_{^{3}H,Q}$ and $C_{\delta^{18}O,^{3}H,Q}$ indicate multi-objective, i.e. simultaneous calibration to combinations of $\delta^{18}O$, ^{3}H and stream flow. The TTD metrics represent the mean and standard deviations of all daily streamflow TTDs during the modelling period 01/10/2001 – 31/12/2016 are given. The mean transit time for each precipitation zone was estimated by fitting Gamma distributions to the volume-weighted mean TTDs. The water fractions are shown as the fractions of below a specific age T. *Note that the fraction of water younger than 3 months is comparable to the fraction of young water as suggested by Kirchner (2016) and the long term-mean precipitation for P1-P4: P2<P3<P1<p4.

	Scenario	19				20				21			
	Calibration strategy	$C_{\delta^{18}O,Q}$				$C_{^{3}H,Q}$				$C_{\delta^{18}O,^{3}H,Q}$			
	Precipitation zone→ TTD metrics ↓	P1	P2	P3	P4	P1	P2	P3	P4	P1	P2	P3	P4
	Mean (yr)	14.5	21.9	15.3	10.2	12.3	21.4	13.0	7.9	12.0	17.7	12.6	8.6
Percentiles (yr)	10^{th}	0.3±0.5	0.4±0.6	0.3±0.5	0.4±0.5	0.3±0.5	0.4±0.7	0.3±0.5	0.3±0.4	0.3±0.4	0.3±0.5	0.3±0.4	0.3±0.4
	25^{th}	2.1±1.6	2.5±2.2	2.1±1.6	2.2±1.2	1.5±1.7	2.0±2.6	1.5±1.7	1.4±1.2	1.5±1.5	1.7±2.0	1.5±1.5	1.6±1.3
	50^{th} (median)	8.4±2.4	10.5±3.7	8.5±2.6	7.2±1.7	6.7±3.6	9.3±6.1	6.7±3.7	5.4±2.1	6.5±3.4	8.1±4.7	6.5±3.4	5.7±2.5
	75^{th}	19.6±2.5	25.8±3.7	20.6±2.8	15.1±1.7	17.1±4.0	25.4±6.8	18.6±4.5	12.4±2.2	17.0±3.8	22.3±5.7	17.6±4.2	13.2±2.6
	90^{th}	30.6±3.8	31.4±4.4	31.0±4.2	25.0±1.9	29.7±4.0	31.3±4.4	30.2±4.2	21.3±2.2	29.0±3.8	31.1±4.4	29.7±4.1	22.6±2.6
Water fractions (%)	F(T<3 m)*	15±9	17±11	16±10	12±8	20±12	22±15	20±13	16±11	21±14	23±15	21±15	17±13
	F(T<6 m)	19±11	21±12	20±11	15±9	26±15	29±18	27±16	22±13	26±16	28±17	27±16	22±15
	F(T<1 yr)	22±11	23±12	22±11	19±9	30±16	32±18	30±16	26±13	29±15	30±17	29±16	25±14
	F(T<3 yr)	30±10	29±11	31±10	30±8	37±14	36±17	37±14	37±11	37±14	36±15	37±14	36±12
	F(T<5 yr)	38±9	35±10	38±9	40±7	44±12	41±15	44±13	48±10	44±12	42±14	45±12	46±11
	F(T<10 yr)	54±7	48±8	54±7	60±6	59±9	51±13	58±10	67±7	60±9	54±11	59±9	65±7
	F(T<20 yr)	75±3	66±5	74±4	84±2	78±5	66±9	76±5	88±2	79±5	71±7	78±5	87±3

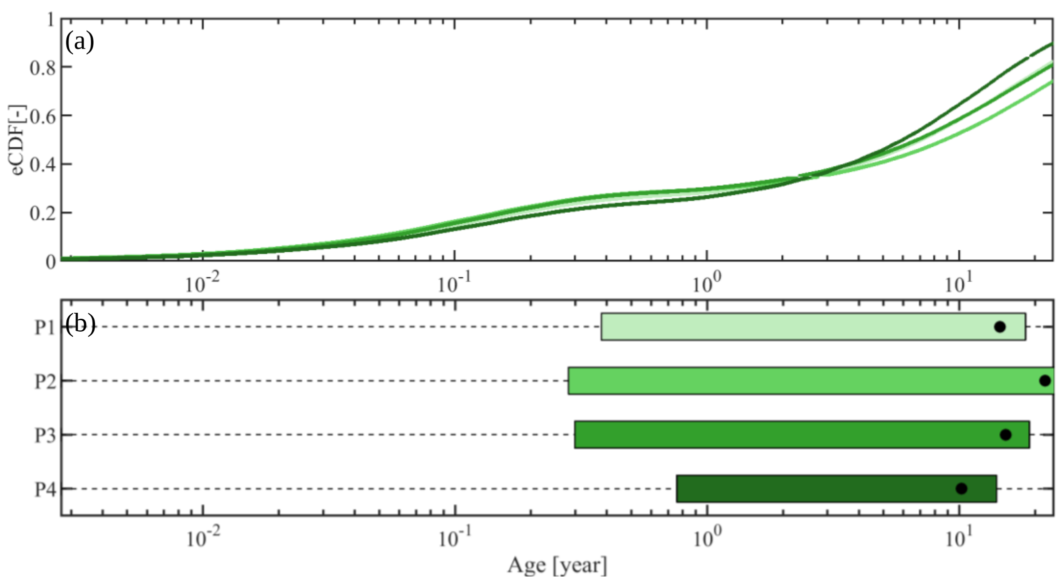

Figure S29. Stream flow weighted-TTDs of four precipitation zones (P1-P4) derived from model scenario19. Different green shades from light to dark represent the TTDs for P1 to P4 in (a) and (b); the black dots in (b) indicate the mean transit time for each precipitation zone. Note that the mean transit time was estimated by fitting Gamma distributions to the volume-weighted mean TTDs of each individual precipitation zone and the long term-mean precipitation for four precipitation zones P1-P4: P2<P3<P1<p4.

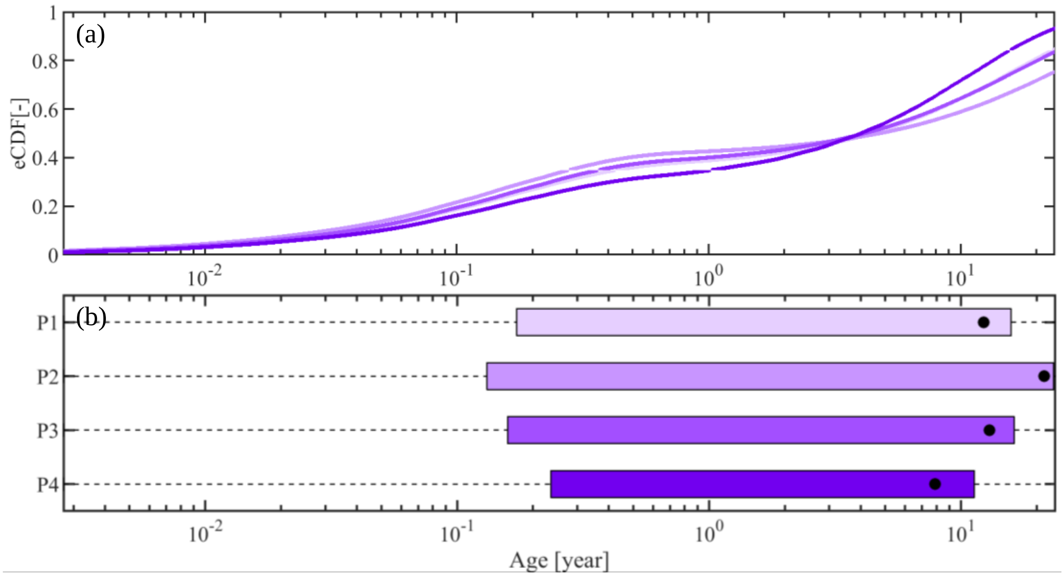

Figure S30. Stream flow weighted-TTDs of four precipitation zones (P1-P4) derived from model scenario20. Different purple shades from light to dark represent the TTDs for P1 to P4 in (a) and (b); the black dots in (b) indicate the mean transit time for each precipitation zone. Note that the mean transit time was estimated by fitting Gamma distributions to the volume-weighted mean TTDs of each individual precipitation zone and the long term-mean precipitation for four precipitation zones P1-P4: P2<P3<P1<p4.

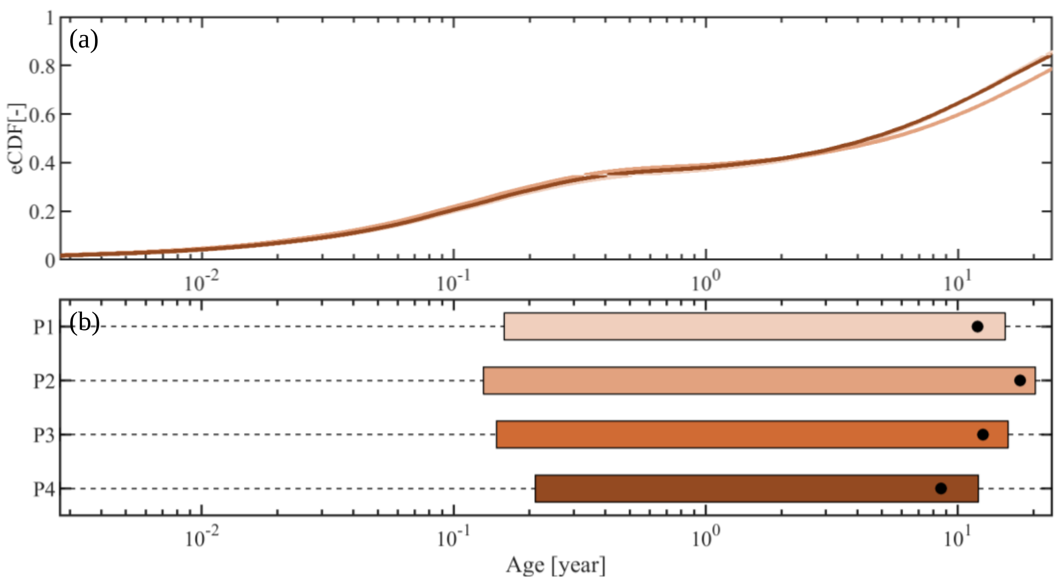

Figure S31. Stream flow weighted-TTDs of four precipitation zones (P1-P4) derived from model scenario21. Different brown shades from light to dark represent the TTDs for P1 to P4 in (a) and (b); the black dots in (b) indicate the mean transit time for each precipitation zone. Note that the mean transit time was estimated by fitting Gamma distributions to the volume-weighted mean TTDs of each individual precipitation zone and the long term-mean precipitation for four precipitation zones P1-P4: P2<P3<P1<p4.

References

Gao, H., Ding, Y., Zhao, Q., Hrachowitz, M., and Savenije, H. H.: The importance of aspect for modelling the hydrological response in a glacier catchment in Central Asia, Hydrol. Process., 31, 2842-2859, https://doi.org/10.1002/hyp.11224, 2017.

Gao, H., Hrachowitz, M., Fenicia, F., Gharari, S., and Savenije, H.: Testing the realism of a topography-driven model (FLEX-Topo) in the nested catchments of the Upper Heihe, China, Hydrol. Earth Syst. Sci., 18, 1895-1915, https://doi.org/10.5194/hess-18-1895-2014, 2014.

Hrachowitz, M., Savenije, H., Bogaard, T., Tetzlaff, D., and Soulsby, C.: What can flux tracking teach us about water age distribution patterns and their temporal dynamics?, Hydrol. Earth Syst. Sci., 17, 533-564, https://doi.org/10.5194/hess-17-533-2013, 2013.

Hrachowitz, M., Stockinger, M., Coenders-Gerrits, M., van der Ent, R., Bogena, H., Lücke, A., and Stumpp, C.: Reduction of vegetation-accessible water storage capacity after deforestation affects catchment travel time distributions and increases young water fractions in a headwater catchment, Hydrol. Earth Syst. Sci., 25, 4887-4915, https://doi.org/10.5194/hess-25-4887-2021, 2021.

Prenner, D., Kaitna, R., Mostbauer, K., and Hrachowitz, M.: The value of using multiple hydrometeorological variables to predict temporal debris flow susceptibility in an alpine environment, Water Resour. Res., 54, 6822-6843, https://doi.org/10.1029/2018WR022985, 2018.